A Tetratricopeptide Repeat Scaffold Couples Signal Detection to OdhI Phosphorylation in Metabolic Control by the Protein Kinase PknG

María-Natalia Lisa, Adrià Sogues, Nathalie Barilone, Meike Baumgart, Magdalena Gil, Martín Graña, Rosario Durán, Ricardo Biondi, Marco Bellinzoni, Michael Bott, et al.

AMERICAN SOCIETY FOR MICROBIOLOGY | mBio®

RESEARCH ARTICLE

A Tetratricopeptide Repeat Scaffold Couples Signal Detection to OdhI Phosphorylation in Metabolic Control by the Protein Kinase PknG

María-Natalia Lisa,[a,b] Adrià Sogues,[a*] Nathalie Barilone,[a§] Meike Baumgart,[c] Magdalena Gil,[d◇] Martín Graña,[e] Rosario Durán,[d] Ricardo M. Biondi,[f†] Marco Bellinzoni,[a] Michael Bott,[c] Pedro M. Alzari[a]

[a]Unité de Microbiologie Structurale, Institut Pasteur, CNRS UMR 3528, Université de Paris, Paris, France
[b]Instituto de Biología Molecular y Celular de Rosario (IBR, CONICET-UNR), Ocampo y Esmeralda, Rosario, Argentina
[c]IBG-1: Biotechnology, Institute of Bio- and Geosciences, Forschungszentrum Jülich, Jülich, Germany
[d]Unidad de Bioquímica y Proteómica Analíticas, Instituto de Investigaciones Biológicas Clemente Estable e Institut Pasteur de Montevideo, Montevideo, Uruguay
[e]Unidad de Bioinformática, Institut Pasteur de Montevideo, Montevideo, Uruguay
[f]Research Group PhosphoSites, Medizinische Klinik 1, Universitätsklinicum Frankfurt, Frankfurt, Germany

ABSTRACT Signal transduction is essential for bacteria to adapt to changing environmental conditions. Among many forms of posttranslational modifications, reversible protein phosphorylation has evolved as a ubiquitous molecular mechanism of protein regulation in response to specific stimuli. The Ser/Thr protein kinase PknG modulates the fate of intracellular glutamate by controlling the phosphorylation status of the 2-oxoglutarate dehydrogenase regulator OdhI, a function that is conserved among diverse actinobacteria. PknG has a modular organization characterized by the presence of regulatory domains surrounding the catalytic domain. Here, we present an investigation using *in vivo* experiments, as well as biochemical and structural methods, of the molecular basis of the regulation of PknG from *Corynebacterium glutamicum* (*Cg*PknG), in the light of previous knowledge available for the kinase from *Mycobacterium tuberculosis* (*Mtb*PknG). We found that OdhI phosphorylation by *Cg*PknG is regulated by a conserved mechanism that depends on a C-terminal domain composed of tetratricopeptide repeats (TPRs) essential for metabolic homeostasis. Furthermore, we identified a conserved structural motif that physically connects the TPR domain to a β-hairpin within the flexible N-terminal region that is involved in docking interactions with OdhI. Based on our results and previous reports, we propose a model in which the TPR domain of PknG couples signal detection to the specific phosphorylation of OdhI. Overall, the available data indicate that conserved PknG domains in distant actinobacteria retain their roles in kinase regulation in response to nutrient availability.

IMPORTANCE Bacteria control the metabolic processes by which they obtain nutrients and energy in order to adapt to the environment. *Actinobacteria*, one of the largest bacterial phyla of major importance for biotechnology, medicine, and agriculture, developed a unique control process that revolves around a key protein, the protein kinase PknG. Here, we use genetic, biochemical, and structural approaches to study PknG in a system that regulates glutamate production in *Corynebacterium glutamicum*, a species used for the industrial production of amino acids. The reported findings are conserved in related *Actinobacteria*, with broader significance for microorganisms that cause disease, as well as environmental species used industrially to produce amino acids and antibiotics every year.

KEYWORDS bacterial signaling, *Corynebacterium glutamicum*, protein kinases, protein structure-function

Citation Lisa M-N, Sogues A, Barilone N, Baumgart M, Gil M, Graña M, Durán R, Biondi RM, Bellinzoni M, Bott M, Alzari PM. 2021. A tetratricopeptide repeat scaffold couples signal detection to OdhI phosphorylation in metabolic control by the protein kinase PknG. mBio 12:e01717-21. https://doi.org/10.1128/mBio.01717-21.

Editor Richard Gerald Brennan, Duke University School of Medicine

Address correspondence to María-Natalia Lisa, lisa@ibr-conicet.gov.ar, or Pedro M. Alzari, pedro.alzari@pasteur.fr.

* Present address: Adrià Sogues, Structural and Molecular Microbiology, VIB-VUB Centre for Structural Biology, Brussels, Belgium.

§Present address: Nathalie Barilone, Unité Récepteurs-Canaux, Institut Pasteur, Paris, France.

◇Present address: Magdalena Gil, Dynamics of Host-Pathogen Interactions Unit, Institut Pasteur, CNRS UMR3691, Paris, France.

†Present address: Ricardo M. Biondi, Instituto de Investigación en Biomedicina de Buenos Aires (IBioBA)-CONICET-Partner Institute of the Max Planck Society, Buenos Aires, Argentina.

Received 11 June 2021
Accepted 7 September 2021
Published 5 October 2021

The large and ancient bacterial phylum *Actinobacteria* comprises species with very diverse lifestyles and physiological adaptations, including soil inhabitants, pathogens, and plant or animal commensals (1). The Hanks-type Ser/Thr protein kinase (STPK) PknG and its FHA (ForkHead-Associated) substrate OdhI (Oxoglutarate dehydrogenase Inhibitor) are at the core of a conserved signal transduction pathway that modulates central metabolism in distant actinobacteria. Both in *Corynebacterium glutamicum*, a soil bacterium used for the industrial production of amino acids, and in the pathogen *Mycobacterium tuberculosis*, PknG modulates the 2-oxoglutarate dehydrogenase activity in the Krebs cycle (2–4) by controlling the phosphorylation status of the regulator OdhI (called GarA in the genus *Mycobacterium*) (2–5). Biochemical studies have demonstrated that unphosphorylated OdhI/GarA inhibits the E1 component (OdhA) of the 2-oxoglutarate dehydrogenase complex, whereas this inhibition is relieved by OdhI/GarA phosphorylation by PknG (2–4, 6, 7). Moreover, early studies for the two species revealed that *pknG* disruption leads to an accumulation of intracellular glutamate (2, 8), pointing out that PknG acts by promoting catabolism at the expense of 2-oxoglutarate usage in nitrogen assimilation. On top of this, it was recently found that PknG is activated, through a sensory relay, by the availability of amino-donor amino acids such as glutamate and aspartate to control metabolism and virulence in *M. tuberculosis* (9–11). These findings have received much attention (10), since a deeper understanding of PknG regulation can be instrumental for downstream applications in the biotech and pharmaceutical areas.

PknG has a unique modular organization characterized by the presence of a highly flexible N-terminal region containing all known autophosphorylation sites and a C-terminal domain composed of tetratricopeptide repeats (TPRs) flanking the kinase catalytic core (12–14). An additional rubredoxin (Rdx)-like domain occurs immediately adjacent to the catalytic core in PknG from mycobacteria and most other actinobacteria, but not in corynebacteria (2). Previous structural studies of PknG have focused on the protein from *M. tuberculosis* (*Mtb*PknG) (12, 13). We have shown that both the N-terminal region and the TPR domain of *Mtb*PknG regulate the selectivity for GarA without significantly affecting the intrinsic kinase activity, whereas the Rdx domain downregulates catalysis by limiting access to a profound substrate-binding site (13). Rdx domains are known to transmit redox stimuli and, consistent with this, evidence has been reported pointing out that perturbations of the metal center in PknG lead to alterations of the kinase activity (15). However, relatively little is known about the regulatory mechanisms of PknG isoforms that lack an Rdx domain.

The gene *pknG* is found within a conserved operon that contains two other genes, *glnX* and *glnH*, which encode a putative transmembrane protein and a putative glutamine-binding lipoprotein, respectively (2, 11). The observation that disruption of any of those genes in *C. glutamicum* led to a similar phenotype consisting of a growth defect in medium containing glutamine as the sole carbon source (2) suggested a common role of the protein products in metabolic homeostasis. Supporting this early hypothesis, evidence has been recently reported that, in mycobacteria, PknG and GlnX are functionally linked and that GlnH specifically binds amino acids able to stimulate GarA phosphorylation by the kinase (11). This led to the proposal that GlnH senses amino acid availability within the bacterial periplasm and transmits this information across the membrane via GlnX to activate PknG by protein-protein interactions (11). Most interesting, a PknG truncation mutant lacking the TPR domain failed to restore the growth defect of a *pknG*-disrupted mycobacterial strain, suggesting that this domain, often involved in protein-protein interactions (16), mediates molecular associations required for the kinase function (11).

To investigate the conservation of mechanisms involved in the regulation of PknG, we studied the kinase isoform from *C. glutamicum* (*Cg*PknG), which is devoid of an Rdx domain. We provide evidence that the C-terminal region of *Cg*PknG, bearing the TPR domain, is crucial for the efficient phosphorylation of OdhI and for the kinase function in metabolic homeostasis. Moreover, our results point out that the recruitment of the

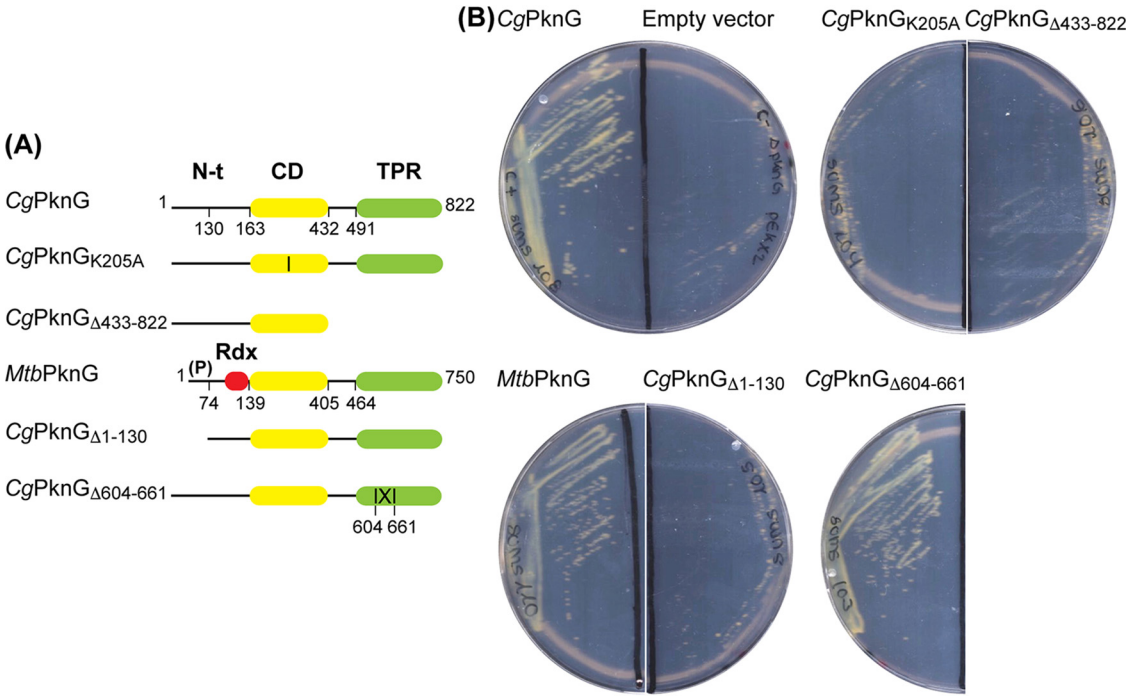

FIG 1 Complementation of the *C. glutamicum* Δ*pknG* mutant (2) with different PknG variants. (A) Schematic representation of the kinase variants tested in complementation assays in this study. The structured domains of the protein are shown as colored rectangles: the Rdx domain in red, the catalytic domain (CD) in yellow, and the TPR domain in green. The vertical line in the CD of mutant *Cg*PknG$_{K205A}$ represents the amino acid substitution. "(P)" indicates the cluster of autophosphorylation sites in the N-terminal region (N-t) of *Mtb*PknG (13). The deletion in the TPR domain of *Cg*PknG$_{\Delta604-661}$ is represented by |X|. (B) Complementation of the Δ*pknG* strain with different *pknG* versions. Complementation was assessed by growth on CGXII plates with 100 mM glutamine as the sole carbon source after 3 days at 30°C. The PknG variants able to complement the Δ*pknG* strain were *Cg*PknG, *Mtb*PknG, and *Cg*PknG$_{\Delta604-661}$. The empty pEKEx2 vector was used as a negative control.

FHA substrate is regulated by a conserved phosphorylation-dependent mechanism regardless of the absence of an Rdx domain. Finally, by comparing three high-resolution crystal structures of *Cg*PknG and an available structure of *Mtb*PknG (12), we identified a conserved motif able to link the N-terminal region with the TPR domain. Interestingly, the evidence suggests that the Rdx domain, absent in corynebacteria, and the TPR domain would constitute independent regulatory mechanisms. Overall, our results indicate that common PknG domains in distant actinobacteria share similar functions in kinase regulation, linking PknG to the control of central metabolism in response to nutrient availability.

RESULTS

The C-terminal region of *Cg*PknG is required for phosphorylation events that modulate metabolism. To investigate the domains required for the function of *Cg*PknG, we employed a previously characterized *C. glutamicum* Δ*pknG* mutant strain able to grow in rich medium but unable to grow in medium containing glutamine as the sole carbon source (2). *Cg*PknG domain boundaries were defined based on a previous characterization of *Mtb*PknG (13) (47% amino acid identity), and plasmids were designed for the expression of *Cg*PknG truncation mutants (Fig. 1A) in *C. glutamicum* Δ*pknG* using the endogenous gene promoter. All strains grew normally in medium containing glucose and all versions of the kinase were detected by Western blotting (see Fig. S1 in the supplemental material).

The active site mutant *Cg*PknG$_{K205A}$ did not complement the growth defect of the *C. glutamicum* Δ*pknG* mutant on glutamine (Fig. 1B). A similar phenotype was shown by the *C. glutamicum* Δ*odhI* strain expressing OdhI$_{T14A}$ (2), indicating that the PknG-dependent phosphorylation of OdhI is required for growth on glutamine as a sole carbon source. In addition, a *Cg*PknG truncation mutant lacking residues 433 to 822 was

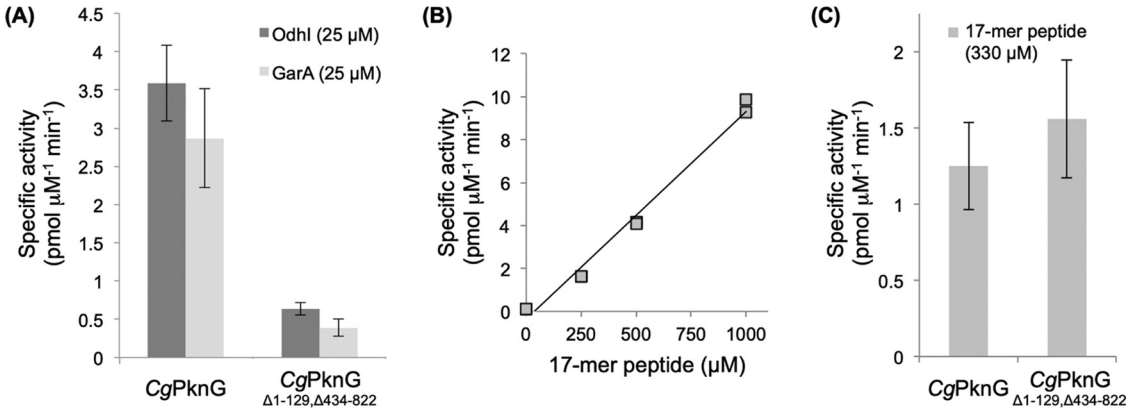

FIG 2 Relative kinase activities of *Cg*PknG and *Cg*PknG$_{\Delta 1\text{-}129,\Delta 434\text{-}822}$. (A) Relative kinase activities of *Cg*PknG and *Cg*PknG$_{\Delta 1\text{-}129,\Delta 434\text{-}822}$ against OdhI and GarA. (B) Kinase activity of *Cg*PknG for different concentrations of the 17-mer peptide substrate SDEVTV**ETTS**VFRADFL. (C) Relative kinase activity of *Cg*PknG and *Cg*PknG$_{\Delta 1\text{-}129,\Delta 434\text{-}822}$ against the 17-mer peptide. Measurements were performed at least twice; error bars represent the scattering among average values obtained in independent determinations.

unable to restore bacterial growth on glutamine, suggesting, in agreement with previous results in *Mycobacterium smegmatis* (11), that the TPR domain of *Cg*PknG is necessary for the kinase role in the control of metabolism. Moreover, *Mtb*PknG did complement the growth defect of the *C. glutamicum* Δ*pknG* strain, stressing the functional conservation between distant kinase isoforms. In contrast, a *Cg*PknG deletion mutant devoid of the first 130 residues, roughly corresponding to the structurally disordered N-terminal segment in the *Mtb*PknG crystal structure (12), failed to restore the growth of the *C. glutamicum* Δ*pknG* strain on glutamine. However, this kinase variant was very poorly expressed in the complemented strain (see Fig. S1), so we were unable to draw a sound conclusion from this observation. Together, these results support the hypothesis that the conserved TPR domain of PknG is required for phosphorylation events that modulate metabolism in response to amino acid availability.

Conserved phosphorylation-dependent mechanism for substrate recruitment. To investigate the molecular mechanisms of metabolic control by the kinase activity of *Cg*PknG, we first tested the ability of recombinant *Cg*PknG to phosphorylate OdhI and GarA *in vitro*. *Cg*PknG phosphorylated OdhI and GarA to a similar extent (Fig. 2A), confirming the ability of *Cg*PknG to phosphorylate both proteins and evidencing that structural differences between OdhI and GarA (4, 17), either in the FHA domain or in the N-terminal phosphorylatable region, do not influence the kinase activity. Moreover, *Cg*PknG phosphorylated GarA in the same peptide as *Mtb*PknG (3) (see Fig. S2). This peptide contains the phosphorylatable residue Thr21 equivalent to OdhI Thr14 phosphorylated by *Cg*PknG (2).

The structurally disordered N-terminal extension of *Mtb*PknG contains several autophosphorylation sites (Thr23, Thr32, Thr63, and Thr64) (3) (Fig. 1A; see also Fig. S3) that act as essential anchoring points for the recruitment of GarA by interacting with the pThr-binding FHA domain of the regulator (3, 13). Since the N-terminal sequence of PknG is poorly conserved (see Fig. S3), we sought to determine whether the equivalent N-terminal region of *Cg*PknG plays a similar role in the recruitment of the FHA substrate. Although no phosphorylation was detected in the purified recombinant protein, four phosphorylation sites (Thr14, Thr68, Thr92, and Thr93) were identified by mass spectrometry (MS) within the N-terminal region of *Cg*PknG after incubating the kinase with ATP and Mn(II) (see Fig. S3 and S4).

We next studied the ability of *Cg*PknG to phosphorylate a substrate lacking an FHA domain, using for this the previously reported 17-mer SDEVTV**ETTS**VFRADFL peptide (13) centered around the phosphorylatable ETTS motif that is conserved among OdhI/GarA homologs (2). The kinase activity of *Cg*PknG varied linearly with the concentration of the 17-mer peptide up to 1 mM, indicating a high K_m (>1 mM) and the slope providing a

TABLE 1 Crystallographic data collection and refinement statistics[a]

Parameter	*Cg*PknG	*Cg*PknG$_{\Delta 1\text{-}129,\Delta 434\text{-}822}$_1	*Cg*PknG$_{\Delta 1\text{-}129,\Delta 434\text{-}822}$_2
Data collection			
Space group	$P2_1$	$P2_12_12_1$	$P2_12_12_1$
Cell dimensions			
a, *b*, *c* (Å)	104.66, 42.74, 175.33	37.62, 55.94, 123.94	37.81, 54.59, 146.49
α, β, γ (°)	90.00, 95.31, 90.00	90.00, 90.00, 90.00	90.00, 90.00, 90.00
Resolution (Å)	46.68–2.20 (2.24–2.20)[a]	41.52–1.92 (1.97–1.92)	48.83-1.99 (2.04–1.99)
R_{merge}	0.086 (0.514)	0.070 (0.746)	0.067 (0.654)
$I/\sigma I$	9.9 (2.0)	13.6 (1.9)	17.1 (2.3)
$CC_{1/2}$	0.996 (0.675)	0.999 (0.805)	0.999 (0.751)
Completeness (%)	99.1 (90.8)	99.9 (100.0)	98.4 (84.9)
Redundancy	3.4 (2.6)	5.9 (5.6)	6.0 (5.2)
Refinement			
Resolution (Å)	43.02–2.20	41.52–1.92	43.77–1.99
No. of reflections	78,937	20,701	21,183
R_{work}/R_{free}	0.210/0.246	0.199/0.225	0.209/0.237
No. of atoms			
Protein	10,369	2,190	2,255
Ligands	68	33	33
Solvent	910	237	157
Avg *B*-factors (Å^2)			
Protein	37.82	32.46	47.67
Ligands	24.54	30.19	33.21
Solvent	38.11	36.72	42.30
RMSD			
Bond length (Å)	0.002	0.003	0.003
Bond angle (°)	0.54	0.63	0.59
Ramachandran (%)			
Favored	98.17	97.85	97.57
Allowed	1.83	2.15	2.43
Outliers	0	0	0
PDB code	7MXB	7MXJ	7MXK

[a]One protein crystal was employed for structure determination in each case. Values in parentheses are for the highest-resolution shell.

measure of the catalytic efficiency (k_{cat}/K_m) of (9.0 ± 0.4) 10^{-3} pmol μM^{-2} min^{-1} for this substrate (Fig. 2B). By comparison, the phosphorylation of OdhI by *Cg*PknG was ~3-fold higher than for the 17-mer peptide even though an ~15-fold-lower concentration of OdhI was used (Fig. 2A and C), indicating an ~45-fold-higher activity toward OdhI due to the FHA domain acting as a kinase docking site (7, 13).

Finally, we tested the kinase activity of a *Cg*PknG deletion mutant lacking residues 1 to 129 and 434 to 822. *Cg*PknG$_{\Delta 1\text{-}129,\Delta 434\text{-}822}$ displayed an ~7-fold-lower activity against OdhI compared to the full-length enzyme, whereas phosphorylation of the 17-mer substrate was unaffected (Fig. 2A and C). These results indicate that neither residues 1 to 129 within the N-terminal region nor the TPR domain of *Cg*PknG has an effect on the intrinsic kinase activity, supporting previous evidence for *Mtb*PknG (13) that both regions contribute to stabilize the enzyme-FHA substrate complex.

Overall, our results indicate that PknG isoforms from different bacteria use a conserved phosphorylation-dependent mechanism to recruit the FHA substrate OdhI (or GarA).

Conserved overall topology. To investigate the structural basis of the regulation of a PknG isoform lacking an Rdx domain, we solved a high-resolution crystal structure of *Cg*PknG in complex with the nonhydrolyzable ATP analog AMP-PNP (Table 1). The final atomic model contains two copies of *Cg*PknG within the asymmetric unit, encompassing residues 123 to 799 and 125 to 798, respectively, including a short fragment of the N-terminal region, the kinase catalytic core and the TPR domain (Fig. 3 and Fig. S5A). The absence of extensive protein-protein interactions in the crystal structure

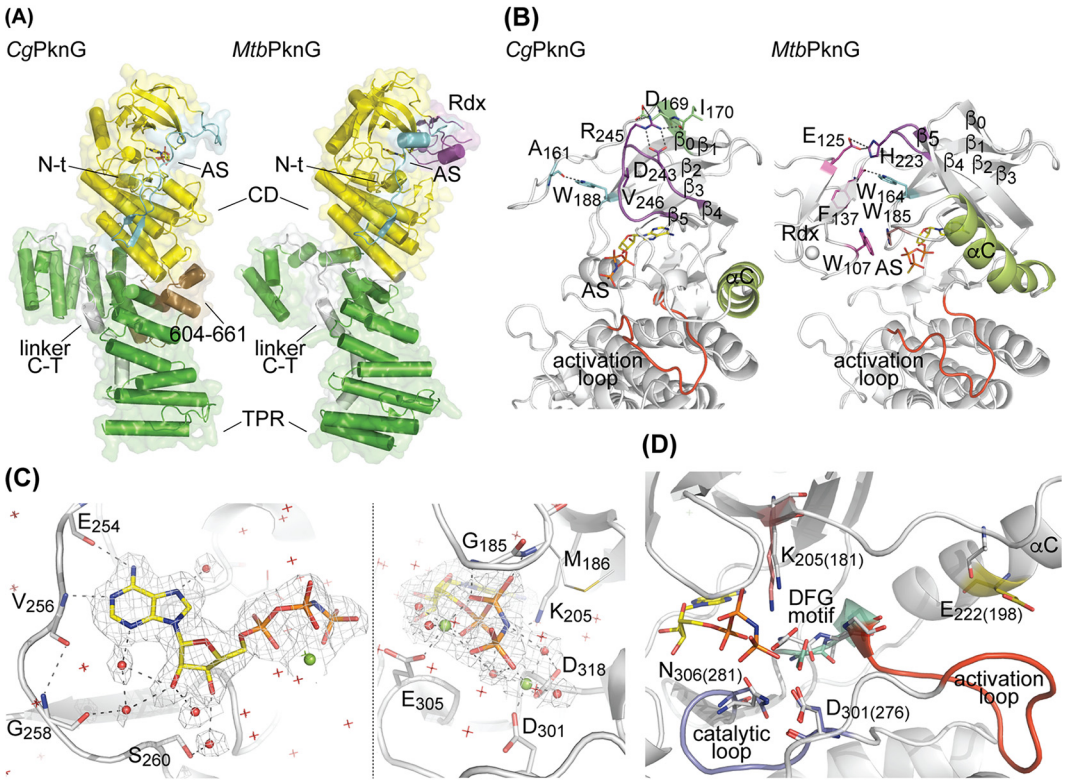

FIG 3 The crystal structure of *Cg*PknG. (A) Comparison of *Cg*PknG and *Mtb*PknG $_{\Delta 1\text{-}73}$ (12) (PDB code 2PZI). The chain A in each crystal structure is shown (RMSD of 2.35 Å for 532 aligned residues). The nonhydrolyzable ATP analog AMP-PNP bound to the active site (AS) of *Cg*PknG is depicted in sticks. The N-terminal region (N-t) is shown in blue, the rubredoxin-like domain (Rdx) in red, the catalytic domain (CD) in yellow, the linker between the catalytic domain, the TPR domain (linker C-T) in white, and the TPR domain in green. The insertion within the *Cg*PknG TPR domain (residues 604 to 611) is shown in orange. (B) Comparison of *Cg*PknG and *Mtb*PknG$_{\Delta 1\text{-}73,\Delta 406\text{-}750}$ (13) (PDB 4Y12). The highlighted kinase domain residues or motifs adopt distinct conformations in the absence or in the presence of an Rdx domain. (C) The ATP binding site of *Cg*PknG with a bound AMP-PNP molecule. The AMP-PNP molecule and the protein residues interacting with it are shown as sticks. Water molecules are depicted as red spheres or stars and Mg(II) atoms are shown as green spheres. The *2mFo–DFc* electron density is contoured to 1.0 σ and presented as a mesh. Dashed lines represent atomic interactions. (D) Functionally important and conserved residues within the kinase active site are shown for *Cg*PknG. Gray sticks correspond to residues in *Mtb*PknG$_{\Delta 1\text{-}73,\Delta 406\text{-}750}$ (13) (PDB 4Y12), numbered between parentheses.

suggests that the protein is monomeric in solution, in agreement with analytical ultracentrifugation data (see Fig. S5B). In addition, *mFo–DFc* sigma-A-weighted electron density maps clearly revealed the bound nucleotide and two Mg(II) atoms at the active site of each *Cg*PknG molecule. Notably, even though we used full-length *Cg*PknG in our crystallization assays, we found no evidence for residues 1 to 122 in electron density maps. Edman degradation experiments revealed that the N-terminal residue of crystallized *Cg*PknG was Val123, suggesting that the kinase N-terminal segment was partially degraded during crystal growth and that, as similarly reported for *Mtb*PknG (12), it is probably unstructured in most of its length.

*Cg*PknG and *Mtb*PknG (12) share the same overall fold and topology, except for the absence of a regulatory Rdx domain in *Cg*PknG that leads to a more accessible active site (Fig. 3A). As expected, kinase domain residues or motifs involved in contacts with the Rdx domain in *Mtb*PknG (12, 13) adopt distinct conformations in *Cg*PknG (Fig. 3B). Residue Trp188 in *Cg*PknG (equivalent to Trp164 in *Mtb*PknG), located in the β_2 strand and adjacent to the G-rich loop, interacts with the N-terminal segment. The loop connecting strands β4 and β5 (loop β4-β5) is found in *Cg*PknG in close association with the kinase N-lobe, with residue Val246 (His223 in *Mtb*PknG) buried within a pocket and residues Asp243 and Arg245 in contact with the strand β0. In addition, the helix αC does not interact with strands β4 and β5 and its C-terminal tip is displaced, in *Cg*PknG compared to *Mtb*PknG, toward the kinase activation loop.

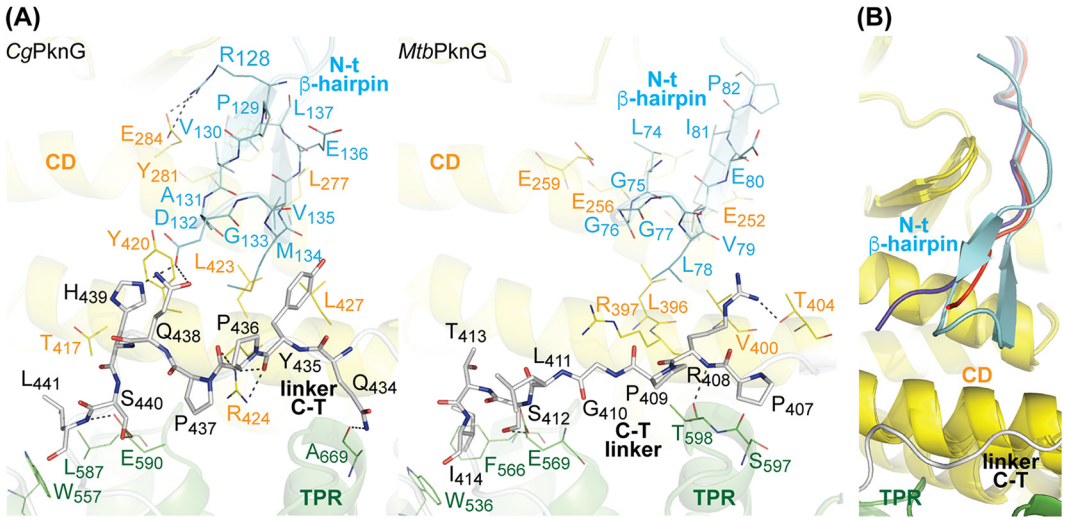

FIG 4 The linker C-T simultaneously interacts with an N-terminal β-hairpin, the catalytic core, and the TPR domain of PknG. (A) Comparison of the crystal structures of *Cg*PknG (this work) and *Mtb*PknG$_{\Delta 1\text{-}73}$ (12) (PDB 2PZI). Chain A in each crystal structure is shown. Selected residues within the linker C-T are shown as sticks. Residues conforming the N-terminal β-hairpin in each structure (residues 128 to 137 in *Cg*PknG and residues 74 to 82 in *Mtb*PknG) are depicted as lines. Residues of the catalytic core or the TPR domain involved in polar or hydrophobic interactions with the N-terminal β-hairpin or the linker C-T are also shown as lines. Dashed lines represent polar interactions. (B) The crystal structures of *Cg*PknG and *Cg*PknG$_{\Delta 1\text{-}129,\Delta 434\text{-}822}$ are superimposed. The root mean square deviation (RMSD) values between the chain A in the structure of *Cg*PknG and the two structures of *Cg*PknG$_{\Delta 1\text{-}129,\Delta 434\text{-}822}$ are 1.04 and 0.79 Å for 282 and 288 aligned residues, respectively. The N-terminal region of *Cg*PknG$_{\Delta 1\text{-}129,\Delta 434\text{-}822}$ is colored in blue or red.

Regardless of these differences, nucleotide binding within the active site of *Cg*PknG parallels the previous description for *Mtb*PknG (13) (Fig. 3C), consistent with a conserved set of residues within the ATP binding site region of the kinase. Also similar to *Mtb*PknG (12, 13), most functionally important and conserved motifs in the active site of *Cg*PknG exhibit conformations compatible with a standard eukaryotic protein kinase active state, and the activation loop is stabilized in an open and extended conformation, permissive for substrate binding in the absence of phosphorylation (Fig. 3D). Nevertheless, *Cg*PknG residue Glu222 is found away from the catalytic Lys205, pointing out of the active site due to an outward conformation of the helix αC, as previously reported for *Mtb*PknG (12, 13).

Compared to *Mtb*PknG, *Cg*PknG contains an insertion (residues 604 to 661) in the TPR domain, adjacent to the catalytic core (Fig. 1 and Fig. 3A). However, a *Cg*PknG truncation mutant lacking these residues (*Cg*PknG$_{\Delta 604\text{-}661}$) did complement the growth defect of *C. glutamicum* Δ*pknG* on glutamine (Fig. 1B), suggesting that this motif is not crucial for the kinase function.

A conserved motif connects the N-terminal segment and the TPR domain. The TPR domain of *Mtb*PknG influences the FHA substrate selectivity and we have previously proposed that this depends on the stabilization of a β-hairpin in the N-terminal region of the kinase (13). In spite of sequence divergence, this secondary structure motif is conserved in *Cg*PknG (Fig. 4A). In both *Cg*PknG and *Mtb*PknG the N-terminal β-hairpin is stabilized by interactions with the catalytic core and the linker between this and the TPR domain (linker C-T comprising residues 433 to 490; see Fig. 1A and 3A). Notably, the linker C-T simultaneously contacts the N-terminal segment, the catalytic core and the TPR domain of the kinase. To explore the significance of such interactions, we solved the high-resolution crystal structures of the truncation mutant *Cg*PknG$_{\Delta 1\text{-}129,\Delta 434\text{-}822}$ in two different isoforms (Table 1). According to the electron density maps, the N-terminal β-hairpin loop (residues 131 to 134) was not stabilized in any of these two structures (Fig. 4B), suggesting that this motif might be responsive to the C-terminal region of the kinase.

DISCUSSION

The phosphorylation-dependent stabilization of enzyme-substrate complexes is a widespread mechanism among STPKs that enables the efficient phosphorylation of specific cellular targets (18). PknG controls metabolism in corynebacteria and mycobacteria by modulating the phosphorylation status of the FHA regulator OdhI (or GarA) (2, 9), a task that requires the N-terminal extension of the kinase. Despite the relatively high sequence divergence of this segment, it has a roughly conserved distribution of charged amino acids and Pro and Gly residues in diverse species (see Fig. S3) and comprises autophosphorylation sites both in *Cg*PknG and in *Mtb*PknG (3) (see Fig. S3 and S4). The N-terminal extension of PknG is dispensable for the phosphorylation of a surrogate peptide lacking an FHA domain (Fig. 2C) (13) and, conversely, the presence of the FHA domain in OdhI or GarA enables a much more efficient phosphorylation by full-length PknG (Fig. 2A and C) (13). Overall, our results support a conserved autophosphorylation-dependent mechanism for the recruitment of the FHA substrate *via* the kinase N-terminal extension.

Kinase domain motifs that play regulatory roles in eukaryotic protein kinases (ePKs) adopt different conformations in PknG isoforms depending on the presence or the absence of an Rdx domain. In *Cg*PknG the loop β4-β5 fills the pocket formed by the β-sheet in the kinase N-lobe, whereas this loop is exposed to the solvent in *Mtb*PknG (12, 13) (Fig. 3B). The pocket and the motifs that may fill it (i.e., the N-lobe cap) lay on top of the catalytic Lys and are features associated with the regulation of ePKs (19). Moreover, the helix αC, an important regulatory motif in ePKs (20, 21), is displaced in *Cg*PknG toward the kinase activation loop compared to *Mtb*PknG (12, 13) (Fig. 3B). Consistent with previous findings for ePKs (22), the crystal structures of both *Cg*PknG and *Mtb*PknG (12, 13) exhibit relatively high B-factors for the loop β3-αC and the N-terminal end of the helix αC, indicating that this motif is highly dynamic. Interestingly, while the Rdx domain in *Mtb*PknG restraints the position of the helix αC by interacting with the loop β3-αC (12, 13), the position adopted by the helix αC in *Cg*PknG generates a pocket that is reminiscent of the PIF-pocket in AGC kinases (22, 23) (see Fig. S6). However, irrespective of the structural differences noted between *Cg*PknG and *Mtb*PknG (13), the ATP phosphates are properly positioned in both kinase isoforms in the active site despite the absence of a salt bridge between the conserved Glu in the helix αC and the catalytic Lys, while other conserved catalytically relevant motifs exhibit conformations compatible with an ePK active state (20) (Fig. 3C and D). Thus far, there is no evidence revealing regulatory mechanisms that depend exclusively on motifs within the kinase catalytic domain. The Rdx module of *Mtb*PknG (absent in *Cg*PknG) remains the sole regulatory element known to modulate the intrinsic activity of PknG (13, 15). It is worth noting that Rdx-mediated regulation appears to act independently of the modulation of substrate specificity by FHA-mediated docking interactions.

Since the assembly of new domain combinations into complex proteins is linked to speciation and segregation into distinct phylogenetic groups (24, 25), we performed a phylogenetic analysis of PknG orthologs to seek for hints about the PknG-Rdx association (see Fig. S7). In line with such a notion, PknG orthologs, distinguished by their unique domain organization, are broadly distributed within *Actinobacteria* and, at the same time, mostly restricted to this bacterial phylum. A homologue of *Mtb*PknG is, however, found in *Ktedonobacter racemifer*. This Gram-positive spore-forming bacterium belongs to *Chloroflexi* and grows in filamentous colonies similarly to a number of actinobacteria (26). *Chloroflexi* is an ancient phylum proposed to be at or very close to the root of the bacterial phylogenetic tree (27). Besides, a readily detectable homologue of PknG from *K. racemifer* is that from *Calothrix* sp. from the ancient phylum *Cyanobacteria*. The fact that both PknG homologues harbor an Rdx domain (defined by the presence of a PknG_rubred Pfam PF16919 domain or two CxxCG motifs) suggests that such domain architecture either preceded the evolution of *Actinobacteria*, being then differentially lost in some lineages, or that the gene of an Rdx-containing PknG homolog was horizontally transferred to *Chloroflexi* and *Cyanobacteria*. We favor the

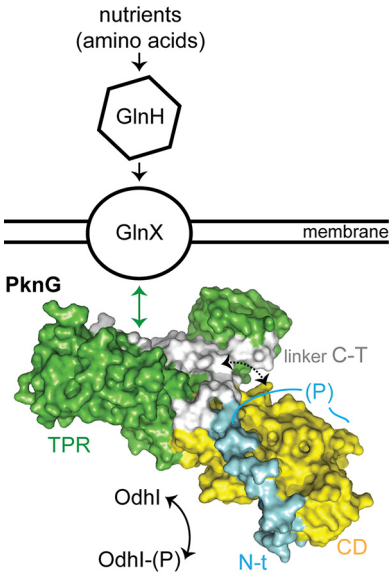

FIG 5 Proposed model for the role of the TPR domain in the *Cg*PknG function. The available genetic, biochemical, and structural evidence suggests that the TPR domain might act as a localization scaffold that, providing a surface for the interaction between the kinase and the transmembrane protein GlnX, would couple signal detection to OdhI phosphorylation by modulating the conformation of the linker C-T.

former, more parsimonious hypothesis because several nonactinobacterial ancient sequences include an Rdx domain, and within *Actinobacteria* only the genus *Corynebacterium* lacks the module. It remains enigmatic why the Rdx domain was lost in the evolution of this genus.

The overall topology of PknG is conserved irrespective of the presence or the absence of an Rdx domain (Fig. 3A). The relative position of the TPR and the catalytic domain of *Cg*PknG is similar to that of *Mtb*PknG (12). Compared to the mycobacterial isoform, *Cg*PknG contains an intriguing insertion of 58 amino acids (residues 604 to 661) within the TPR domain (Fig. 1A and Fig. 3A) that increases its interface with the catalytic core. However, our *in vivo* tests suggested that this insertion is not essential for the role of *Cg*PknG in metabolic homeostasis (Fig. 1B). In contrast, the TPR domain of *Cg*PknG (residues 433 to 822) was required for complementing the *C. glutamicum* Δ*pknG* mutant strain (Fig. 1B), replicating previous results in *M. smegmatis* (11) and pointing to a conserved role of the TPR domain in signal transduction. Notably, in *Cg*PknG as in *Mtb*PknG the linker C-T bridges the N-terminal segment and the TPR domain (Fig. 4A) (12), both regions involved in the regulation of the kinase selectivity for the FHA substrate (13). The linker C-T is stabilized by conserved interactions with residues along the concave surface of the TPR domain (Fig. 3A) (12). According to a recent proposal (11), this surface might constitute a binding site for GlnX, so that the transduction of extracellular stimuli would imply a conformational change of the linker C-T from its position in the free form of the kinase.

Taking together the available evidence, we propose that the TPR domain of PknG functions as a localization scaffold that, by mediating an interaction between the kinase and the transmembrane protein GlnX, transduces a signal about amino acid availability detected by GlnH (Fig. 5). The PknG-GlnX interaction likely produces a conformational change in the linker C-T, which couples the detection of the signal to the specific recruitment of the FHA substrate via the N-terminal segment of the kinase. Given that the specific set of multidomain proteins in genomes sets constraint on the topology of pathways and networks that carry out regulatory processes (28), the cooccurrence of *pknG*, *glnX*, *glnH*, and *odhI* in actinobacteria (2, 11), together with the functional links found among the respective proteins, therefore suggests the conservation

TABLE 2 Plasmids used in this study

Plasmid	Description	Source or reference
pEKEx2	KAN^R. Allows the IPTG-inducible production of proteins in *C. glutamicum*.	50
pEKEx2-*pknG*$_{St}$	Kan^r. Derived from pEKEx2. Designed for the production in *C. glutamicum* of C-terminally Strep-tagged full-length *Cg*PknG from the endogenous gene promoter.	2
pEKEx2-*Cg*PknG$_{K205A}$	Kan^r. Derived from pEKEx2-*pknG*$_{St}$. Used for the production in *C. glutamicum* of C-terminally Strep-tagged full-length *Cg*PknG carrying substitution K205.	This study
pEKEx2-*Cg*PknG$_{\Delta 433-822}$	Kan^r. Derived from pEKEx2-*pknG*$_{St}$. Used for the production in *C. glutamicum* of C-terminally Strep-tagged *Cg*PknG lacking residues 433 to 822.	This study
pEKEx2-*Mtb*PknG	Kan^r. Derived from pEKEx2-*pknG*$_{St}$. Used for the production in *C. glutamicum* of C-terminally Strep-tagged full-length *Mtb*PknG.	This study
pEKEx2-*Cg*PknG$_{\Delta 1-130}$	Kan^r. Derived from pEKEx2-*pknG*$_{St}$. Used for the production in *C. glutamicum* of C-terminally Strep-tagged *Cg*PknG lacking residues 1 to 130.	This study
pEKEx2-*Cg*PknG$_{\Delta 604-661}$	Kan^r. Derived from pEKEx2-*pknG*$_{St}$. Used for the production in *C. glutamicum* of C-terminally Strep-tagged *Cg*PknG lacking residues 604 to 661.	This study
pET28a-*Cg*PknG	Kan^r; derived from pET28a. Used for the IPTG-inducible production in *E. coli* of N-terminally His_6-tagged full-length *Cg*PknG.	This study
pET28a-*Cg*PknG$_{\Delta 1-129,\Delta 434-822}$	Kan^R. Derived from pET28a. Used for the IPTG-inducible production in *E. coli* of N-terminally His_6-tagged full-length *Cg*PknG lacking residues 1 to 129 and residues 434 to 822.	This study

of the associated molecular mechanism that evolved in this phylum to control metabolism in response to nutrient availability.

MATERIALS AND METHODS

Complementation assays. All plasmids used in this study are listed in Table 2. Plasmids for complementation assays were generated by Genscript (Leiden, The Netherlands) from the previously described pEKEx2-*pknG*$_{St}$ template plasmid (2). The *C. glutamicum* Δ*pknG* strain (2) was transformed with each of the plasmids carrying the relevant *pknG* variants or with the pEKEx2 vector lacking an insert, as previously described (29). Then, strains were first streaked on brain heart infusion (BHI) medium (BD BBL). In each case, single colonies were subsequently plated both on CGXII-glucose (30) and CGXII-glutamine. The CGXII-glutamine broth is a modified version of medium CGXII that is devoid of $(NH_4)_2SO_4$, urea, and glucose and is supplemented with 100 mM glutamine. Plates were cultivated for 3 days at 30°C.

Detection of PknG versions by Western blotting. Transformed *C. glutamicum* Δ*pknG* (2) cells were grown at 30°C in BHI broth (BD BBL) with agitation until reaching 3 U of optical density at 600 nm. Protein expression was then induced by adding IPTG (isopropyl-β-D-thiogalactopyranoside) to a final concentration of 1 mM, and the incubation was continued for 20 h at 30°C. Cells were then harvested by centrifugation. Cell pellets were suspended in lysis buffer (50 mM Bis-Tris, 75 mM 6-aminocaproic acid, 1 mM $MgSO_4$, 1 U/ml benzonase, cOmplete EDTA-free protease inhibitor cocktail [Roche] in the amount specified by the manufacturer [pH 7.4]) and disrupted by using 0.1-mm glass beads and a homogenizer (Precellys 24) operated at 4°C. Next, 120- to 250-μg portions of protein of crude extracts were run in a precast 4 to 12% SDS-PAGE gradient gel (Bio-Rad) and then electrotransferred onto a 0.2-μm nitrocellulose membrane (Bio-Rad). Blocking was performed with PBS buffer supplemented with 3% (wt/vol) BSA and 0.05% (vol/vol) Tween 20. The membrane was subsequently incubated with an anti-Strep antibody (StrepMAB-Classic; IBA Lifesciences) at 4°C overnight. After three washes with TBS-Tween buffer (10 mM Tris-HCl, 150 mM NaCl, 0.05% [vol/vol] Tween 20 [pH 8.0]) for 5 min for each wash, the membrane was incubated with a secondary anti-rabbit horseradish peroxidase (HRP)-conjugated antibody (GE Healthcare) for 45 min at room temperature. Finally, the membrane was washed three times with TBS-Tween buffer for 5 min each time, visualized with HRP substrate (Immobilon Forte; Millipore), and imaged using the ChemiDoc MP imaging system (Bio-Rad).

Construction of plasmids for the production of recombinant proteins. Plasmids pET28a-*Cg*PknG and pET28a-*Cg*PknG$_{\Delta 1-129,\Delta 434-822}$ (Table 2) were constructed by PCR amplification of *pknG* regions comprising residues 1 to 822 and 130 to 433, respectively, from *C. glutamicum* ATCC 13032 genomic DNA, followed by digestion and ligation of the amplification products into the NdeI and SacI sites in plasmid pET28a (Novagen). The following oligonucleotides were used (the Tobacco Etch Virus protease cleavage sites are underlined): *Cg*PknG-F, ATTATCATATG<u>GAGAATCTTTATTTTCAGGGC</u>ATGAAGGATAATGAAGATTTCG ATCC; *Cg*PknG-R, ATATTGAGCTCTCACTAGAACCAACTCAGTGGCCGCACGGC; Δ1-129,Δ434-822-F, TATATTATCATATG<u>GAGAATCTTTATTTTCAGGGC</u>GTTGCTGATGGCATGGTGGAATTG; and Δ1-129,Δ434-822-R, TATATATTGAGCTCTCATTTGCCGTCGCGGACTGCCAAAATTTC.

Protein production and purification. Wild-type *Cg*PknG and the truncation mutant *Cg*PknG$_{\Delta 1-129,\Delta 434-822}$ were both overproduced in *Escherichia coli* BL21(DE3) cells cultivated in Luria-Bertani (LB) broth. Wild-type *Cg*PknG was produced for 18 h at 15°C with 500 μM IPTG, whereas *Cg*PknG$_{\Delta 1-129,\Delta 434-822}$ was expressed after 3 h of induction at 30°C with 250 μM IPTG. Both proteins were then purified according to the same protocol. *E. coli* cells were harvested by centrifugation, resuspended in lysis buffer (25 mM HEPES, 500 mM NaCl, 20% [vol/vol] glycerol, 20 mM imidazole [pH 8.0]), supplemented with cOmplete EDTA-free protease inhibitor cocktail (Roche) as specified by the manufacturer, and sonicated. After clarification by centrifugation, the supernatant was loaded onto a HisTrap HP column (GE Healthcare), and His-tagged protein was purified,

applying a linear imidazole gradient (20 to 500 mM) in lysis buffer. The His_6 tag was later removed by overnight incubation at 4°C with 0.2 equivalents of His_6-tagged TEV protease, followed by separation on a Ni-NTA agarose column (Qiagen). The protein was then further purified by size exclusion chromatography on a 16/600 Superdex 200 column (GE Healthcare) equilibrated in either 50 mM Tris-HCl–250 mM NaCl–5% glycerol (pH 8.0) (wild type *Cg*PknG) or 25 mM HEPES–150 mM NaCl–5% glycerol (pH 7.5) ($CgPknG_{\Delta 1\text{-}129,\Delta 434\text{-}822}$), using a flow rate of 0.5 to 1 ml/min. Fractions corresponding to *Cg*PknG or $CgPknG_{\Delta 1\text{-}129,\Delta 434\text{-}822}$, as confirmed by SDS-PAGE, were pooled and concentrated, flash-frozen in liquid nitrogen, and stored at −80°C. GarA and OdhI were prepared as previously described (17, 31). Proteins were quantified using the molar absorption coefficient predicted from the amino acid sequence by the ProtParam tool (http://web.expasy.org/protparam/).

Protein kinase activity assays. Kinase activity assays were performed in 96-well plates. Each activity measurement was performed in a final volume of 20 μl, containing 50 mM Tris-HCl (pH 7.4), 0.1% (vol/vol) 2-mercaptoethanol, 10 mM $MnCl_2$, 100 μM [γ-^{32}P]ATP (5 to 50 cpm/pmol), and 330 μM 17-mer peptide or 25 μM OdhI (or GarA) as the substrate. The enzyme concentration in the assays was 0.7 to 3 μM and 0.15 to 0.9 μM when using the 17-mer peptide or OdhI (or GarA) as the substrates, respectively. The kinase reactions were started by the addition of 4 μl of [γ-^{32}P]ATP-Mn^{+2} and were performed at room temperature. The reactions were stopped by the addition of phosphoric acid, and 4 μl of each reaction mixture was spotted onto P81 phosphocellulose papers (Whatman) using an epMotion 5070 (Eppendorf) workstation. The papers were washed in 0.01% phosphoric acid, dried, and then measured and analyzed using a phosphorimager (FLA-9000 Starion; Fujifilm). Each reaction was performed in duplicates (<5% variation). In all cases, specific activity values were derived from reactions performed employing three different enzyme concentrations within the indicated ranges (<10% variation), verifying a linear dependence of activity with the enzyme concentration. Each assay was performed at least twice. The proportion of 17-mer peptide or OdhI (or GarA) phosphorylated in the reactions was lower than 10 or 30%, respectively. OdhI (or GarA) phosphorylation was verified to be linear in time up to 50% of its initial concentration. Under the experimental conditions employed to test phosphorylation of the 17-mer peptide or OdhI (or GarA), *Cg*PknG autophosphorylation represented <5% of the total signal. The measured signal was at least five times higher than the measure on the background. The 17-mer peptide SDEVTV**ETTS**VFRADFL was produced with a purity >98% by Thermo Fisher Scientific.

Mass spectrometry analysis. The kinase activity of *Cg*PknG was assayed using GarA as the substrate, and the molecular mass of unphosphorylated and phosphorylated GarA was then determined as previously described (15).

*Cg*PknG was incubated with ATP and $MnCl_2$ and then sequentially digested with trypsin and endoproteinase GluC for 3 h at 37°C. The resulting peptides were separated using a nano-HPLC system (Proxeon EasynLC; Thermo) with a reversed-phase column (Easy C_{18} column, 3 μm; 75-μm inner diameter × 10 cm; Proxeon; Thermo) and eluted with a 0.1% (vol/vol) formic acid (in water)-to-acetonitrile gradient (0 to 40% acetonitrile in 50 min; flow, 300 nl/min). Online MS analysis was carried out in a linear ion trap instrument (LTQ Velos; Thermo) in data dependent acquisition mode (full scan, followed by MS/MS of the top five peaks in each segment, using a dynamic exclusion list). Raw MS/MS spectra were extracted by the Proteome Discoverer software package (v.1.3.0.339; Thermo) and submitted to Sequest for database searching against sequences from *E. coli* (strain K-12) downloaded from the UniProt consortium (April 2021), to which the sequence of PknG from *C. glutamicum* was added. Search parameters were set as follows: peptide tolerance, 0.8 Da; MS/MS tolerance, 0.8 Da; with methionine oxidation and Ser/Thr/Tyr phosphorylation as the allowed variable modifications. PhosphoRS was used as phospho-site localization tool (32). We considered a positive phospho-site identification when more than one spectrum for the phospho-peptide was obtained, the pRS probability was >95%, and manual inspection of the MS/MS spectra showed at least two confirmatory fragment ions.

Crystallization and data collection. Crystallization screenings were carried out using the sitting-drop vapor diffusion method and a Mosquito nanoliter-dispensing crystallization robot (TTP Labtech). Crystals of *Cg*PknG + AMP-PNP and $CgPknG_{\Delta 1\text{-}129,\Delta 434\text{-}822}$ + AMP-PNP grew after 20 to 30 days and 7 to 10 days, respectively, from 10-mg/ml protein solutions supplemented with 5 mM AMP-PNP, by mixing 200 nl of protein solution and 200 nl of mother liquor (100 mM Tris-HCl, 17% [wt/vol] PEG 20,000, 100 mM $MgCl_2$ [pH 8.5]; and 100 mM Tris-HCl, 27 to 30% [wt/vol] PEG 4,000, 200 mM $MgCl_2$ [pH 8.8], respectively), at 18°C. Single crystals reaching a size of (100 μm)^3 were cryoprotected in mother liquor containing 25% glycerol and flash-frozen in liquid nitrogen. X-ray diffraction data were collected at the synchrotron beamlines Proxima 2 (Synchrotron Soleil, Saint-Aubin, France) and ID29 (ESRF, Grenoble, France) at 100 K. The employed wavelengths were 0.9801 and 0.97625 Å for the *Cg*PknG + AMP-PNP and $CgPknG_{\Delta 1\text{-}129,\Delta 434\text{-}822}$ + AMP-PNP crystals, respectively. The diffraction data were processed using XDS (33) and scaled with Aimless (34) from the CCP4 program suite.

Structure determination and refinement. The crystal structure of *Cg*PknG + AMP-PNP was solved by molecular replacement using the program Phaser (35) and the atomic coordinates of *Mtb*PknG residues 138 to 405 from PDB 4Y0X (13) and residues 406 to 750 from PDB 2PZI (12) as search probes. The structures of $CgPknG_{\Delta 1\text{-}129,\Delta 434\text{-}822}$ + AMP-PNP were solved similarly by using the atomic coordinates of *Cg*PknG residues 165 to 425. Ligand molecules were manually placed in *mFo–DFc* sigma-A-weighted electron density maps employing Coot (36). Models were refined through iterative cycles of manual model building with Coot and reciprocal space refinement with phenix.refine (37). The final models were validated through the MolProbity server (38). In each case, the final model contained more than 97% of residues within favored regions of the Ramachandran plot, with no outliers. Figures were generated and rendered with PyMOL 1.8.x (Schrödinger, LLC).

Edman degradation. The crystal employed to solve the structure of *Cg*PknG was dissolved in water and Edman degradation was performed by the Functional Genomics Center of Zurich (https://fgcz.ch/omics_areas/prot/applications/protein-characterization.html). As a control, an aliquot of the TEV-cleaved purified recombinant *Cg*PknG (as used in crystallization screenings) was also analyzed, and the sequence of the protein N terminus yielded GMKDN, as expected.

Analytical ultracentrifugation. Sedimentation velocity experiments were carried out at 20°C in an XL-I analytical ultracentrifuge (Beckman Coulter). Samples were spun using an An60Ti rotor and 12-mm double sector epoxy centerpieces. The partial specific volume of *Cg*PknG (0.734 ml g^{-1}) was estimated from their amino acid sequences using the software Sednterp. The same software was used to estimate the buffer viscosity (η = 1.040 centipoises) and density (ρ = 1.010 g ml^{-1}). *Cg*PknG (400 μl at 1 mg/ml) was spun at 42,000 rpm, and absorbance profiles were recorded every 5 min. Sedimentation coefficient distributions, c(s), were determined using Sedfit 14.1 software (39).

Database searches, alignments, and phylogenetic analyses. BLASTp searches (40) were conducted against complete protein sequences available at the Integrated Microbial Genome (IMG; http://img.jgi.doe.gov) (41), performing a taxon sampling on finished assembled genomes within the phyla *Cyanobacteria*, *Chloroflexi*, *Chlorobi*, *Fusobacteria*, *Sinergistetes*, *Firmicutes*, *Tenericutes*, *Acidobacteria*, *Nitrospirae*, *Spirochaetes*, *Aquificae*, and *Thermotogae*, all in the vicinity of *Actinobacteria* in an updated tree of life (27). The sequence of *Mtb*PknG was used as queries for searches to identify homologues in such genomes using an expected inclusion threshold E value of $<1\ e^{-20}$. Once the existence of the domain combinations was confirmed, we focused on 91 complete *Actinobacteria* genomes available from IMG (April 2021). The final selection was preprocessed using PREQUAL (42) to mask nonhomologous sequence stretches. A CD-HIT (43) cutoff value of 90% pairwise identity was applied for the entire set of sequences retrieved, as described previously. The final set of 40 sequences was aligned with MAFFT (version 7.467) using the L-INS-I strategy (44), and columns with more than 90% gaps were removed with trimAl (45). The phylogenetic tree displayed in Fig. S7 was computed with IQ-TREE (version 1.6.12) (46) using ModelFinder (47) to select the evolutionary model and the ultrafast bootstrap method (48) (options "-bb 1000 -alrt 1000"). The model selected with the Bayesian Information Criterion was the evolutionary matrix EX_EHO (49) with empirical frequencies and four categories of free rate (EX_EHO+F+R4).

Data availability. Atomic coordinates and structure factors have been deposited in the Protein Data Bank under the accession codes 7MXB (*Cg*PknG + AMP-PNP), 7MXJ (*Cg*PknG$_{\Delta 1\text{-}129,\Delta 434\text{-}822}$ + AMP-PNP_1), and 7MXK (*Cg*PknG$_{\Delta 1\text{-}129,\Delta 434\text{-}822}$ + AMP-PNP_2).

SUPPLEMENTAL MATERIAL

Supplemental material is available online only.

FIG S1, TIF file, 1.6 MB.

FIG S2, TIF file, 0.4 MB.

FIG S3, TIF file, 0.8 MB.

FIG S4, TIF file, 0.6 MB.

FIG S5, TIF file, 1.4 MB.

FIG S6, TIF file, 1.2 MB.

FIG S7, TIF file, 0.5 MB.

ACKNOWLEDGMENTS

M.-N.L. received fellowships from the EMBO (European Molecular Biology Organization) and the Fondation pour la Recherche Médicale (FRM; France). This study was funded by grants from the Institut Pasteur, the CNRS (France), the Agence Nationale de la Recherche (ANR, France, contract ANR-09-BLAN-0400) and the European Commission Seventh Framework Program (contract HEALTH-F3-2011-260872). M.-N.L. acknowledges support from the Agencia I+D+I (grant PICT 2017-1932). R.M.B. acknowledges support from DFG (grant BI 1044/12-1).

We thank Ahmed Haouz and Patrick Weber for help with robot-driven crystallization screenings and Bertrand Raynal for help with analytical ultracentrifugation experiments. We acknowledge William Shepard for assistance in the collection of diffraction data at beamline Proxima 2 and Martin Cohen-Gonsaud for providing plasmid pET-15b-Tev-OdhI for OdhI production.

M.-N.L. designed experiments, prepared proteins, performed kinase activity assays, carried out crystallographic studies and structural analysis, analyzed data, and wrote the paper. A.S. performed complementation assays, analyzed data, and wrote the paper. N.B. generated constructs pET28a-*Cg*PknG and pET28a-*Cg*PknG$_{\Delta 1\text{-}129,\Delta 434\text{-}822}$, optimized the production of recombinant proteins, and performed analytical ultracentrifugation experiments. M.Ba. performed complementation assays and analyzed data. M.Gi. carried out mass spectrometry analyses. M.Gr. performed phylogenetic analysis. R.D. designed

and performed mass spectrometry studies. R.M.B. designed kinase activity assays and analyzed data. M.Be., M.Bo., and P.M.A. designed research and analyzed data. All authors copy edited the paper.

REFERENCES

1. Barka EA, Vatsa P, Sanchez L, Gaveau-Vaillant N, Jacquard C, Meier-Kolthoff JP, Klenk H-P, Clément C, Ouhdouch Y, van Wezel GP. 2016. Taxonomy, physiology, and natural products of actinobacteria. Microbiol Mol Biol Rev 80:1–43. https://doi.org/10.1128/MMBR.00019-15.
2. Niebisch A, Kabus A, Schultz C, Weil B, Bott M. 2006. Corynebacterial protein kinase G controls 2-oxoglutarate dehydrogenase activity via the phosphorylation status of the OdhI protein. J Biol Chem 281:12300–12307. https://doi.org/10.1074/jbc.M512515200.
3. O'Hare HM, Durán R, Cerveñansky C, Bellinzoni M, Wehenkel AM, Pritsch O, Obal G, Baumgartner J, Vialaret J, Johnsson K, Alzari PM. 2008. Regulation of glutamate metabolism by protein kinases in mycobacteria. Mol Microbiol 70:1408–1423. https://doi.org/10.1111/j.1365-2958.2008.06489.x.
4. Nott TJ, Kelly G, Stach L, Li J, Westcott S, Patel D, Hunt DM, Howell S, Buxton RS, O'Hare HM, Smerdon SJ. 2009. An intramolecular switch regulates phosphoindependent FHA domain interactions in *Mycobacterium tuberculosis*. Sci Signal 2:ra12. https://doi.org/10.1126/scisignal.2000212.
5. Ventura M, Rieck B, Boldrin F, Degiacomi G, Bellinzoni M, Barilone N, Alzaidi F, Alzari PM, Manganelli R, O'Hare HM. 2013. GarA is an essential regulator of metabolism in mycobacterium tuberculosis. Mol Microbiol 90:356–366. https://doi.org/10.1111/mmi.12368.
6. Krawczyk S, Raasch K, Schultz C, Hoffelder M, Eggeling L, Bott M. 2010. The FHA domain of OdhI interacts with the carboxy-terminal 2-oxoglutarate dehydrogenase domain of OdhA in *Corynebacterium glutamicum*. FEBS Lett 584:1463–1468. https://doi.org/10.1016/j.febslet.2010.03.028.
7. Wagner T, André-Leroux G, Hindie V, Barilone N, Lisa M-N, Hoos S, Raynal B, Vulliez-Le Normand B, O'Hare HM, Bellinzoni M, Alzari PM. 2019. Structural insights into the functional versatility of an FHA domain protein in mycobacterial signaling. Sci Signal 12:eaav9504. https://doi.org/10.1126/scisignal.aav9504.
8. Cowley S, Ko M, Pick N, Chow R, Downing KJ, Gordhan BG, Betts JC, Mizrahi V, Smith DA, Stokes RW, Av-Gay Y. 2004. The *Mycobacterium tuberculosis* protein serine/threonine kinase PknG is linked to cellular glutamate/glutamine levels and is important for growth *in vivo*. Mol Microbiol 52:1691–1702. https://doi.org/10.1111/j.1365-2958.2004.04085.x.
9. Rieck B, Degiacomi G, Zimmermann M, Cascioferro A, Boldrin F, Lazar-Adler NR, Bottrill AR, Le Chevalier F, Frigui W, Bellinzoni M, Lisa M-N, Alzari PM, Nguyen L, Brosch R, Sauer U, Manganelli R, O'Hare HM. 2017. PknG senses amino acid availability to control metabolism and virulence of *Mycobacterium tuberculosis*. PLoS Pathog 13:e1006399. https://doi.org/10.1371/journal.ppat.1006399.
10. York A. 2017. Bacterial physiology: an inside job on metabolism. Nat Rev Microbiol 15:383–383. https://doi.org/10.1038/nrmicro.2017.68.
11. Bhattacharyya N, Nkumama IN, Newland-Smith Z, Lin LY, Yin W, Cullen RE, Griffiths JS, Jarvis AR, Price MJ, Chong PY, Wallis R, O'Hare HM. 2018. An aspartate-specific solute-binding protein regulates protein kinase G activity to control glutamate metabolism in mycobacteria. mBio 9:e00931-18. https://doi.org/10.1128/mBio.00931-18.
12. Scherr N, Honnappa S, Kunz G, Mueller P, Jayachandran R, Winkler F, Pieters J, Steinmetz MO. 2007. Structural basis for the specific inhibition of protein kinase G, a virulence factor of *Mycobacterium tuberculosis*. Proc Natl Acad Sci U S A 104:12151–12156. https://doi.org/10.1073/pnas.0702842104.
13. Lisa M-N, Gil M, André-Leroux G, Barilone N, Durán R, Biondi RM, Alzari PM. 2015. Molecular basis of the activity and the regulation of the eukaryotic-like S/T protein kinase PknG from *Mycobacterium tuberculosis*. Structure 23:1039–1048. https://doi.org/10.1016/j.str.2015.04.001.
14. Reckel S, Hantschel O. 2015. Kinase regulation in *Mycobacterium tuberculosis*: variations on a theme. Structure 23:975–976. https://doi.org/10.1016/j.str.2015.05.005.
15. Gil M, Graña M, Schopfer FJ, Wagner T, Denicola A, Freeman BA, Alzari PM, Batthyány C, Durán R. 2013. Inhibition of *Mycobacterium tuberculosis* PknG by non-catalytic rubredoxin domain specific modification: reaction of an electrophilic nitro-fatty acid with the Fe-S center. Free Radic Biol Med 65:150–161. https://doi.org/10.1016/j.freeradbiomed.2013.06.021.
16. Zeytuni N, Zarivach R. 2012. Structural and functional discussion of the tetra-trico-peptide repeat, a protein interaction module. Structure 20:397–405. https://doi.org/10.1016/j.str.2012.01.006.
17. Barthe P, Roumestand C, Canova MJ, Kremer L, Hurard C, Molle V, Cohen-Gonsaud M. 2009. Dynamic and structural characterization of a bacterial FHA protein reveals a new autoinhibition mechanism. Structure 17:568–578. https://doi.org/10.1016/j.str.2009.02.012.
18. Jin J, Pawson T. 2012. Modular evolution of phosphorylation-based signaling systems. Philos Trans R Soc Lond B Biol Sci 367:2540–2555. https://doi.org/10.1098/rstb.2012.0106.
19. Thompson EE, Kornev AP, Kannan N, Kim C, Ten Eyck LF, Taylor SS. 2009. Comparative surface geometry of the protein kinase family. Protein Sci 18:2016–2026. https://doi.org/10.1002/pro.209.
20. Huse M, Kuriyan J. 2002. The conformational plasticity of protein kinases. Cell 109:275–282. https://doi.org/10.1016/s0092-8674(02)00741-9.
21. Kornev AP, Taylor SS. 2010. Defining the conserved internal architecture of a protein kinase. Biochim Biophys Acta 1804:440–444. https://doi.org/10.1016/j.bbapap.2009.10.017.
22. Hindie V, Stroba A, Zhang H, Lopez-Garcia LA, Idrissova L, Zeuzem S, Hirschberg D, Schaeffer F, Jørgensen TJD, Engel M, Alzari PM, Biondi RM. 2009. Structure and allosteric effects of low-molecular-weight activators on the protein kinase PDK1. Nat Chem Biol 5:758–764. https://doi.org/10.1038/nchembio.208.
23. Leroux AE, Biondi RM. 2020. Renaissance of allostery to disrupt protein kinase interactions. Trends Biochem Sci 45:27–41. https://doi.org/10.1016/j.tibs.2019.09.007.
24. Vogel C, Bashton M, Kerrison ND, Chothia C, Teichmann SA. 2004. Structure, function and evolution of multidomain proteins. Curr Opin Struct Biol 14:208–216. https://doi.org/10.1016/j.sbi.2004.03.011.
25. Han JH, Batey S, Nickson AA, Teichmann SA, Clarke J. 2007. The folding and evolution of multidomain proteins. Nat Rev Mol Cell Biol 8:319–330. https://doi.org/10.1038/nrm2144.
26. Cavaletti L, Monciardini P, Bamonte R, Schumann P, Rohde M, Sosio M, Donadio S. 2006. New lineage of filamentous, spore-forming, gram-positive bacteria from soil. Appl Environ Microbiol 72:4360–4369. https://doi.org/10.1128/AEM.00132-06.
27. Castelle CJ, Banfield JF. 2018. Major new microbial groups expand diversity and alter our understanding of the Tree of Life. Cell 172:1181–1197. https://doi.org/10.1016/j.cell.2018.02.016.
28. Zmasek CM, Godzik A. 2012. This déjà vu feeling-analysis of multidomain protein evolution in eukaryotic genomes. PLoS Comput Biol 8:e1002701. https://doi.org/10.1371/journal.pcbi.1002701.
29. van der Rest ME, Lange C, Molenaar D. 1999. A heat shock following electroporation induces highly efficient transformation of *Corynebacterium glutamicum* with xenogeneic plasmid DNA. Appl Microbiol Biotechnol 52:541–545. https://doi.org/10.1007/s002530051557.
30. Frunzke J, Engels V, Hasenbein S, Gätgens C, Bott M. 2008. Co-ordinated regulation of gluconate catabolism and glucose uptake in *Corynebacterium glutamicum* by two functionally equivalent transcriptional regulators, GntR1 and GntR2. Mol Microbiol 67:305–322. https://doi.org/10.1111/j.1365-2958.2007.06020.x.
31. England P, Wehenkel A, Martins S, Hoos S, André-Leroux G, Villarino A, Alzari PM. 2009. The FHA-containing protein GarA acts as a phosphorylation-dependent molecular switch in mycobacterial signaling. FEBS Lett 583:301–307. https://doi.org/10.1016/j.febslet.2008.12.036.
32. Taus T, Köcher T, Pichler P, Paschke C, Schmidt A, Henrich C, Mechtler K. 2011. Universal and confident phosphorylation site localization using phosphoRS. J Proteome Res 10:5354–5362. https://doi.org/10.1021/pr200611n.
33. Kabsch W. 2010. XDS. Acta Crystallogr D Biol Crystallogr 66:125–132. https://doi.org/10.1107/S0907444909047337.
34. Evans PR, Murshudov GN. 2013. How good are my data and what is the resolution? Acta Crystallogr D Biol Crystallogr 69:1204–1214. https://doi.org/10.1107/S0907444913000061.
35. McCoy AJ, Grosse-Kunstleve RW, Adams PD, Winn MD, Storoni LC, Read RJ. 2007. Phaser crystallographic software. J Appl Crystallogr 40:658–674. https://doi.org/10.1107/S0021889807021206.
36. Emsley P, Lohkamp B, Scott WG, Cowtan K. 2010. Features and development of Coot. Acta Crystallogr D Biol Crystallogr 66:486–501. https://doi.org/10.1107/S0907444910007493.

37. Afonine PV, Grosse-Kunstleve RW, Echols N, Headd JJ, Moriarty NW, Mustyakimov M, Terwilliger TC, Urzhumtsev A, Zwart PH, Adams PD. 2012. Towards automated crystallographic structure refinement with phenix.refine. Acta Crystallogr D Biol Crystallogr 68:352–367. https://doi.org/10.1107/S0907444912001308.
38. Williams CJ, Headd JJ, Moriarty NW, Prisant MG, Videau LL, Deis LN, Verma V, Keedy DA, Hintze BJ, Chen VB, Jain S, Lewis SM, Arendall WB, Snoeyink J, Adams PD, Lovell SC, Richardson JS, Richardson DC. 2018. MolProbity: more and better reference data for improved all-atom structure validation. Protein Sci 27:293–315. https://doi.org/10.1002/pro.3330.
39. Schuck P. 2000. Size-distribution analysis of macromolecules by sedimentation velocity ultracentrifugation and Lamm equation modeling. Biophys J 78:1606–1619. https://doi.org/10.1016/S0006-3495(00)76713-0.
40. Altschul SF, Madden TL, Schäffer AA, Zhang J, Zhang Z, Miller W, Lipman DJ. 1997. Gapped BLAST and PSI-BLAST: a new generation of protein database search programs. Nucleic Acids Res 25:3389–3402. https://doi.org/10.1093/nar/25.17.3389.
41. Markowitz VM, Chen IMA, Palaniappan K, Chu K, Szeto E, Grechkin Y, Ratner A, Jacob B, Huang J, Williams P, Huntemann M, Anderson I, Mavromatis K, Ivanova NN, Kyrpides NC. 2012. IMG: the integrated microbial genomes database and comparative analysis system. Nucleic Acids Res 40:D115–D122. https://doi.org/10.1093/nar/gkr1044.
42. Whelan S, Irisarri I, Burki F. 2018. PREQUAL: detecting non-homologous characters in sets of unaligned homologous sequences. Bioinformatics 34:3929–3930. https://doi.org/10.1093/bioinformatics/bty448.
43. Li W, Godzik A. 2006. Cd-hit: a fast program for clustering and comparing large sets of protein or nucleotide sequences. Bioinformatics 22:1658–1659. https://doi.org/10.1093/bioinformatics/btl158.
44. Katoh K, Toh H. 2008. Recent developments in the MAFFT multiple sequence alignment program. Brief Bioinform 9:286–298. https://doi.org/10.1093/bib/bbn013.
45. Capella-Gutiérrez S, Silla-Martínez JM, Gabaldón T. 2009. trimAl: a tool for automated alignment trimming in large-scale phylogenetic analyses. Bioinformatics 25:1972–1973. https://doi.org/10.1093/bioinformatics/btp348.
46. Minh BQ, Schmidt HA, Chernomor O, Schrempf D, Woodhams MD, von Haeseler A, Lanfear R. 2020. IQ-TREE 2: new models and efficient methods for phylogenetic inference in the genomic era. Mol Biol Evol 37:1530–1534. https://doi.org/10.1093/molbev/msaa015.
47. Kalyaanamoorthy S, Minh BQ, Wong TKF, Von Haeseler A, Jermiin LS. 2017. ModelFinder: fast model selection for accurate phylogenetic estimates. Nat Methods 14:587–589. https://doi.org/10.1038/nmeth.4285.
48. Hoang DT, Chernomor O, von Haeseler A, Minh BQ, Vinh LS. 2018. UFBoot2: Improving the Ultrafast Bootstrap Approximation. Mol Biol Evol 35:518–522. https://doi.org/10.1093/molbev/msx281.
49. Le SQ, Gascuel O. 2010. Accounting for solvent accessibility and secondary structure in protein phylogenetics is clearly beneficial. Syst Biol 59:277–287. https://doi.org/10.1093/sysbio/syq002.
50. Eikmanns BJ, Kleinertz E, Liebl W, Sahm H. 1991. A family of *Corynebacterium glutamicum*/*Escherichia coli* shuttle vectors for cloning, controlled gene expression, and promoter probing. Gene 102:93–98. https://doi.org/10.1016/0378-1119(91)90545-m.